Geomechanics and Engineering, *Vol. 36, No. 1 (2024) 1-8*
https://doi.org/10.12989/gae.2024.36.1.001

Void detection for tunnel lining backfill using impact-echo method based on continuous wavelet transform and convolutional neural network

Jiyun Lee[1a], Kyuwon Kim[2b], Meiyan Kang[1c], Eun-Soo Hong[2d] and Suyoung Choi*[1]

[1]*Department of Mathematics, Ajou University, 206, World cup-ro, Yeongtong-gu, Suwon-si, Gyeonggi-do, Republic of Korea*
[2]*HBC, Inc., 138, Dunsanjung-ro, Seo-gu, Daejeon, Republic of Korea*

(*Received December 15, 2022, Revised November 5, 2023, Accepted November 10, 2023*)

Abstract. We propose a new method for detecting voids behind tunnel concrete linings using the impact-echo method that is based on continuous wavelet transform (CWT) and a convolutional neural network (CNN). We first collect experimental data using the impact-echo method and then convert them into time–frequency images via CWT. We provide a CNN model trained using the converted images and experimentally confirm that our proposed model is robust. Moreover, it exhibits outstanding performance in detecting backfill voids and their status.

Keywords: continuous wavelet transform; convolutional neural network; impact-echo method; lining backfill; nondestructive testing; void detection

1. Introduction

Impact-echo is a nondestructive method of testing concrete structures. It utilizes impact-generated stress (sound) waves (Sansalone and Streett 1997) that propagate through concrete and are reflected by internal flaws and external surfaces. This method has been utilized for concrete backfill void diagnoses.

During tunnel construction, the lack of backfill material in the void between a tunnel segment lining and the ground can increase the water pressure, thereby deteriorating the stability of the tunnel structure and nearby ground.

In addition, water leakage as a result of lack of backfill material is one of the most important problems in the operational stages of the tunnel (Gong *et al.* 2019). Many researchers have been studied factors for tunnel lining stability (Xu *et al.* 2020, Liu *et al.* 2020, Moon *et al.* 2022, Mirzaeiabdolyousefi *et al.* 2020), but there are only a few trials for detecting backfill voids located behind the tunnel lining.

Research into the application of the impact echo method to backfill analyses on tunnel segments has recently been conducted (Aggelis *et al.* 2008, Song and Cho 2009, 2010, Yao *et al.* 2018, Cao *et al.* 2019). However, these analyses involve an expert performing qualitative analysis; thus, their interpretation is subjective.

Recently, the advancement of data-driven technologies has led to the application of AI technology in various fields, including civil engineering (Lee *et al.* 2022, Kwak and Ko 2022, Sasmal and Behera 2021). Simply implementing AI technology is insufficient for achieving top-tier model performance. To reach that level, it's crucial to rigorously explore various methods for data preprocessing and hyperparameter optimization. Additionally, a solid mathematical foundation is indispensable for further improving model efficacy.

In this study, an AI algorithm combined with the signal analysis is proposed for interpreting the impact-echo backfill data.

The signals obtained via the impact-echo method contain a lot of noise, which must be removed during void detection. However, the dependence on expert experience increases the failure rate for void detection. This study aims to propose a method for analyzing the signals associated with the impact-echo method without performing noise removal.

The time–frequency image of the time series shows the distribution of the signal in both the time and frequency domains, which can supply a wealth of information for void detection. The continuous wavelet transform (CWT) is one of the most useful techniques for converting a one-dimensional signal to two-dimensional time–frequency images. The converted images can then be analyzed using a convolutional neural network (CNN), which is a popular deep learning method for analyzing visual imagery (He *et al.* 2016).

Recently, the method of evolving CWT and CNN by convergence has been highlighted in various fields (Liao *et al.* 2017). In this study, we propose an efficient method for concrete backfill void detection using the impact-echo method based on a combination of CWT and CNN.

*Corresponding author, Professor
E-mail: schoi@ajou.ac.kr
[a]M.S.
E-mail: leejystar@ajou.ac.kr
[b]M.S.
E-mail: romyykim@gmail.com
[c]Ph.D. Student
E-mail: miyeon@ajou.ac.kr
[d]Ph.D.
E-mail: esh6750@nate.com

http://www.techno-press.org/?journal=gae&subpage=7
ISSN: 2005-307X (Print), 2092-6219 (Online)

We produced concrete three test specimens and collected 3137 experimental data points using the impact-echo method. Each datum is labeled as (A), concrete with a solid backfill layer but liable to boundary effects; (B), concrete with a solid backfill layer; or (C), concrete with an insufficient backfill layer.

We normalized the data and converted them into time–frequency images via CWT. We built a CNN model with only two convolutional layers to classify the images converted from the impact-echo signals into the (A), (B), and (C) categories.

Surprisingly, our model was robust, and it achieved an accuracy of more than 0.96 despite not including any noise removal steps. We also demonstrated that our model is superior to the 1D-CNN method that does not utilize CWT conversion.

2. Analysis of time-voltage data

The impact-echo method is one of the most popular nondestructive testing methods for detecting defects in concrete structures using stress waves (the most successful application of the method is the use of mechanical shocks to generate stress pulses). The impact on the surface produces high-energy pulses that can penetrate deep into concrete to detect internal defects and are reflected at the boundary of the internal defects or external boundaries (Sawicki *et al.* 2021, Carino 2001). The pulse signal is recorded by the oscilloscope as time–voltage data whenever the waves return to the surface and is captured by the receiver (accelerometer), as shown in Fig. 1.

Voids within the concrete are detected by analyzing reflected waves. The interaction of stress waves with voids results in specific changes in amplitude, frequency, or time delay in the reflected wave pattern, indicating the void's presence and characteristics. Evaluating these patterns in recorded data allows precise localization of voids within the concrete structure, enabling comprehensive assessment of concrete integrity and quality, and facilitating timely maintenance and essential repairs. Furthermore, we aim to enhance void detection by applying the Continuous Wavelet Transform (CWT) to the recorded data, further refining the method's effectiveness.

CWT is one of the most advanced tools for analyzing signal data for efficiently determining the damping ratio of oscillating signals (Slavic *et al.* 2003). Moreover, it is resistant to noise in the signal. If a function $\varphi(t)$ contained in $L^2(\mathbb{R})$ exists and if its Fourier transform $\hat{\varphi}(\omega)$ satisfies

$$\int_0^\infty \frac{|\hat{\varphi}(\omega)|^2}{\omega}\, d\omega < \infty,$$

then $\varphi(t)$ is called a *wavelet basis*.

A wavelet basis can be scaled to analyze the high- and low-frequency components of the signal while simultaneously performing a convolution over time. A *wavelet function* is a function obtained from a wavelet basis via scaling (with a scale parameter α) and shifting (with a shift parameter β) as

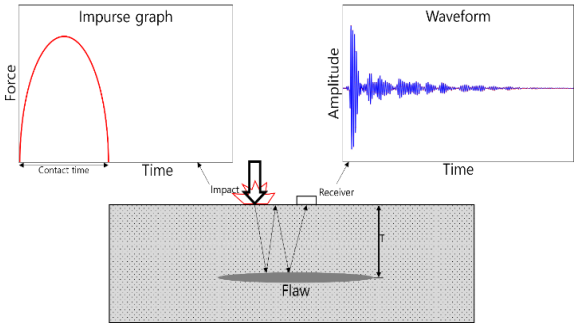

Fig. 1 Schematic of the impact-echo method

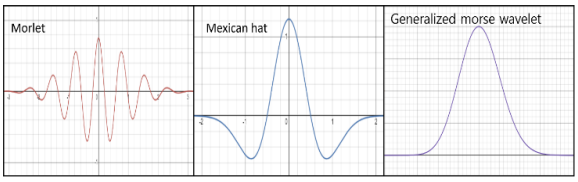

Fig. 2 Types of wavelet functions

$$\varphi_{\alpha,\beta}(t) = \frac{1}{\sqrt{\alpha}}\varphi\left(\frac{t-\beta}{\alpha}\right)$$

The CWT $W_{x(t)}(\alpha,\beta)$ of signal $x(t)$ using a wavelet function $\varphi_{\alpha,\beta}(t)$ is defined as

$$W_{x(t)}(\alpha,\beta) = \int_{-\infty}^{\infty} x(t)\cdot\varphi_{\alpha,\beta}(t)\, dt$$

Convolution of the signal while continuously changing the scale parameters of the wavelet provides an image with detailed information about the time, scale, and amplitude. Accordingly, a method of preprocessing time series data with CWT is applicable to the signal classification problem.

Different wavelet functions, namely, Morlet, Mexican hat, and Generalized Morse wavelet (GMW) are presented in Fig. 2.

Among the aforementioned wavelet functions, GMW exhibited the best performance in this study. Indeed, GMW is commonly used in wavelet analysis (Lilly and Olhede 2012, 2009, 2010), and GMW is defined as follows (Lilly 2017).

Let $U(\omega)$ be the Heaviside step function and $a_{\tau,\gamma} \equiv 2\left(\frac{e\gamma}{\tau}\right)^{\frac{\tau}{\gamma}}$ be a real-valued normalizing constant function. Then, GMW is a function $\psi_{\tau,\gamma}(t)$ defined as

$$\psi_{\tau,\gamma}(t) = \frac{1}{2\pi}\int_{-\infty}^{\infty} \Psi_{\tau,\gamma}(\omega)e^{i\omega t}\, d\omega$$

where $\Psi_{\tau,\gamma}(\omega) = U(\omega)a_{\tau,\gamma}\omega^{\tau}e^{-\omega^{\gamma}}$. The parameter τ controls the low-frequency behavior, whereas γ controls the high-frequency decay.

3. Convolutional neural networks

In this section, we discuss the use of CNNs for classifying

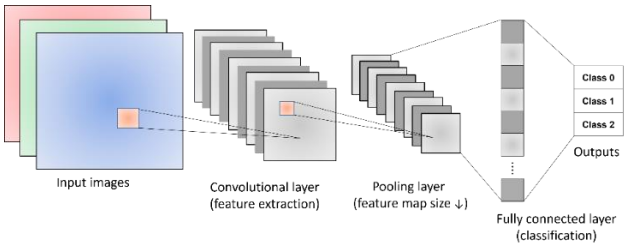

Fig. 3 Full CNN process

images pre-processed with CWT. A CNN architecture is formed by a stack of a few distinct layers that transform inputs into outputs. Fig. 3 shows a simple CNN model consisting of convolutional, pooling, and fully connected layers.

3.1 Convolutional layer

The convolution layer extracts features from the image through a filter, and each additional convolution layer extracts more complex features than that before. Features are extracted from an image using a small matrix called a *filter*. The filter multiplies and moves each pixel to calculate the entire image, forming a feature map in the output layer.

3.2 Pooling layer

The pooling layer can reduce the total number of parameters of the CNN model and the size of the feature map, thereby increasing the computational efficiency of the neural network. Typical examples include max pooling and average pooling.

3.3 Fully connected layer

The fully connected layer is responsible for classifying images by connecting the last output feature map of the convolutional/pooling layer in one-dimensional vector form. We calculated this one-dimensional vector with weights as a linear combination and added activation functions and biases to create vectors with the same number and size of labels. We then applied the SoftMax function to this vector.

4. Data preparation

4.1 Data collection

The experimental setup included three concrete specimens, each constructed from the same material used for tunnel inner walls. These specimens contained a hidden Styrofoam layer measuring 400 × 400 × 400 mm, representing an insufficient backfill layer situated at depths of 200 mm, 300 mm, and 450 mm from each specimen's surface. To achieve an Unconfined Compressive Strength (UCS) of 15-20 MPa, we adjusted the ratios of cement, aggregates, and water. Although the study aimed to measure a 1000 mm × 1000 mm cross-section in a single assessment, the specimens were deliberately designed with a 2000 mm

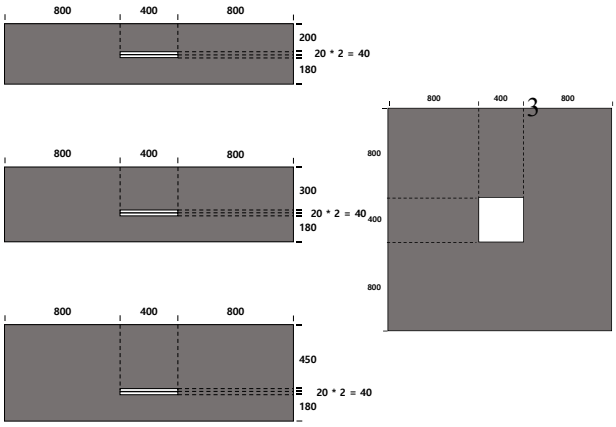

Fig. 4 Full Concrete specimens

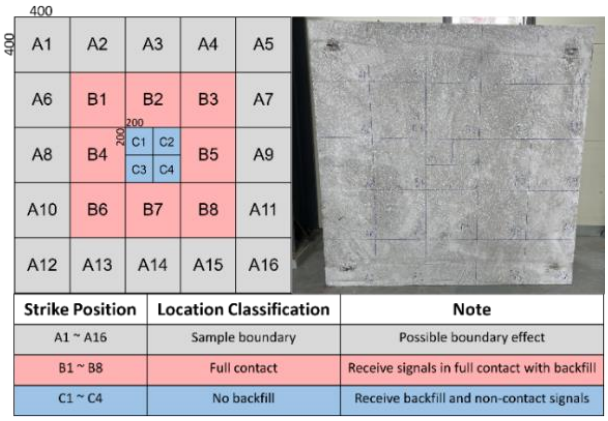

Fig. 5 Impact position of the concrete test specimens

Fig. 6 Mechanical shock

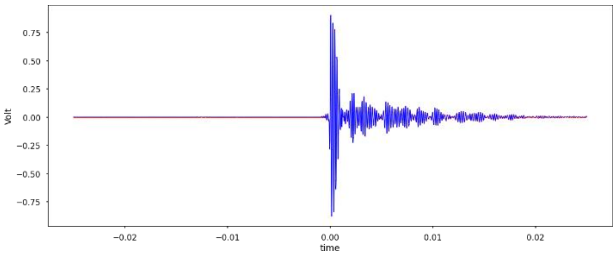

Fig. 7 Graphs of data obtained using the oscilloscope

× 2000 mm cross-sectional area to mitigate any boundary effects that might occur.

The concrete test specimens are shown in Figs. 4 and 5.

We produced impact signals using a steel ball which uses a solenoid device to impact the surface of specimens, as shown in Fig. 6. The generated data were then collected.

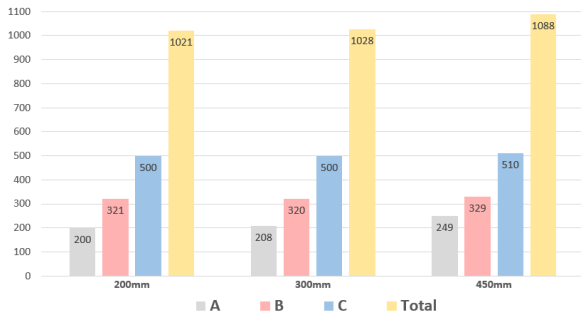

Fig. 7 Graphs of data obtained using the oscilloscope

Table 1 Descriptive data statistics

Data(Voltage)	Mean	STD*	Min	Med	Max
200(A+B+C)	-0.016	0.067	-1.021	-0.016	1.021
200A	-0.024	0.067	-1.021	-0.020	1.021
200B	-0.017	0.068	-1.021	-0.016	1.021
200C	-0.013	0.067	-1.021	-0.012	1.021
300(A+B+C)	-0.013	0.112	-1.685	-0.015	1.685
300A	-0.013	0.134	-1.685	-0.009	1.685
300B	-0.013	0.096	-1.685	-0.013	1.685
300C	-0.013	0.111	-1.685	-0.019	1.685
450(A+B+C)	-0.016	0.131	-2.378	-0.018	2.728
450A	-0.025	0.113	-2.378	-0.018	2.725
450B	-0.012	0.145	-2.378	-0.013	2.728
450C	-0.013	0.130	-2.378	-0.022	2.728

*STD: Standard deviation of the data; Med: Median of the data

A customized gun was used to create the impact. Notably, the impact position of the concrete specimens was randomly selected to prevent data regularity.

The data from areas A, B, and C were collected at a ratio of 2:3:5 for each test specimen. The collected data contain information on voltage and time, as shown in Fig. 7.

Noticeably, Fig. 7 shows a slight change even after a substantial change in the voltage at t = 0. This is attributable to the principle underlying the impact-echo method. The vibration, which is produced by applying an external impact with a force capable of reaching the inside of the test specimen, is reflected by an internal defect or the opposite outer wall. Accordingly, the vibration inside the test specimen meets and amplifies the reflected vibration, generating noise that changes the voltage value even after impact.

4.2 Data statistics

The number of data points for each test specimen is shown in Fig. 8.

The descriptive statistics for the voltage values are listed in Table 1.

5. Data analysis

5.1 L1 normalization

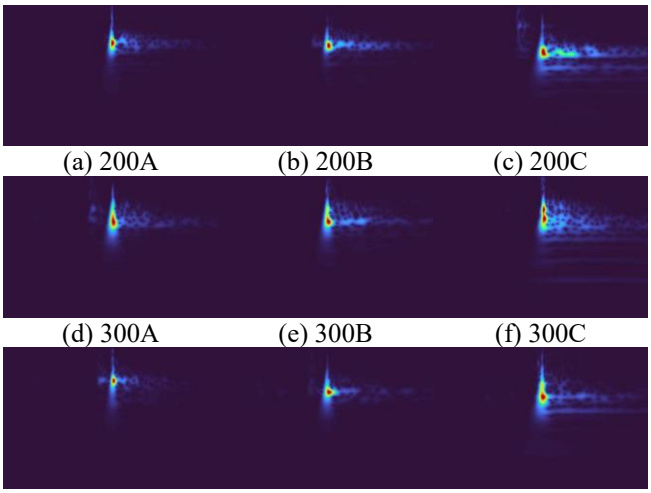

(a) 200A (b) 200B (c) 200C

(d) 300A (e) 300B (f) 300C

(g) 450A (h) 450B (i) 450C

Fig. 9 Images generated using wavelets of A, B, and C

To reduce the influence of environmental conditions on the signals, data normalization is required. The L1 norm was used to normalize the amplitudes of all frequencies to the same value instead of reducing the high-frequency amplitude by multiplying the Fourier transform by $\frac{1}{\alpha}$ (Lilly 2017).

$$\int_{-\infty}^{\infty} x(t) \cdot \frac{1}{\alpha} \varphi\left(\frac{t-\beta}{\alpha}\right) dt$$

Fig. 9 shows the sample images of the CWT image normalized by the L1 norm.

In the samples labeled A and B, where no voids exist, only minimal or weakly reflected waves are observed. In contrast, in the samples labeled C, which contain voids, the impact wave is reflected by these voids, leading to a noticeable increase in amplitude. Consequently, when analyzing the Continuous Wavelet Transform (CWT) of the samples C, as shown in Fig. 9, an elevated amplitude can be observed, extending to the right from the center.

5.2 Results and comparison

Using the CWT image as input data, we adjusted the hyperparameters of the CNN model and checked its performance. First, the optimal wavelet function is essential for achieving good CNN model performance. We considered five wavelet functions: Morlet (morl), Complex Mexican Hat (cmh), Bump (bump), Hilbert analytic function of Hermitian hat (hhhat), and Generalized Morse Wavelet (gmw).

Fig. 10 shows that using GMW as the wavelet function yielded the best performance. We then determined the optimal experimental conditions by adjusting the hyperparameters of the CNN model (number of layers and filters, dropout, etc.). In addition, to prevent unbalanced data learning, we applied stratified five-fold cross-validation to learn all the data at least once. The entire data set was divided into training and test data at a ratio of 7:3, and a stratified five-fold was applied to the training data, as shown in Fig. 11.

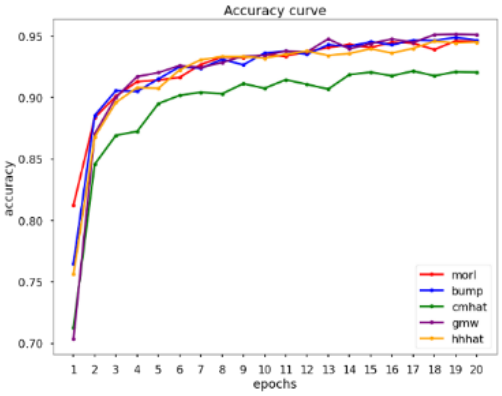

(a) Accuracy curve

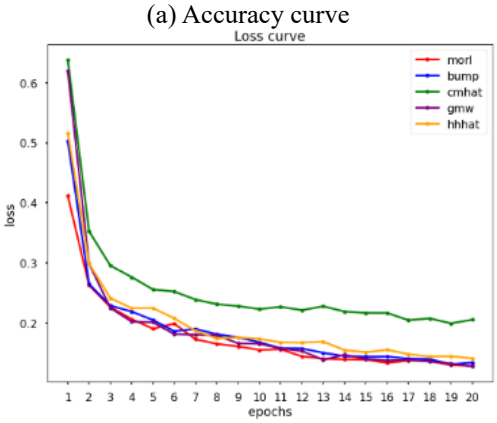

(b) Loss curve

Fig. 10 CNN Model performance for different wavelets

Fig. 11 Stratified five-fold cross-validation

We implemented the CNN model using Python libraries TensorFlow and pycwt. During the data preprocessing phase, we applied CWT via the pycwt library to generate images, such as the one depicted in Fig. 9. Subsequently, we used TensorFlow to fine-tune the filter size, number of layers, pooling method, and other hyperparameters, resulting in the optimal CNN model structure outlined in Table 2.

We compare the aforementioned with 1D-CNN, a time-series analysis method, to validate the usefulness of the CWT images. We then evaluated whether the learning model appropriately classified the test data.

To obtain the trust of the indicators, it is necessary to check whether learning has progressed appropriately by inspecting the learning curves shown in Figs. 12 and 13.

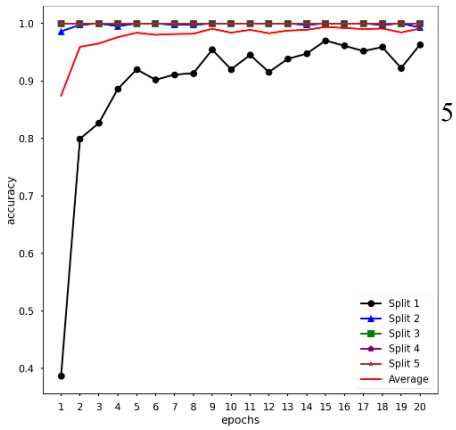

(a) Accuracy curve with (A), (B), and (C)

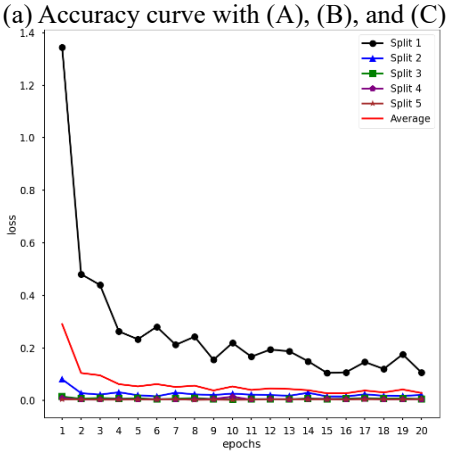

(b) Loss curve with (A), (B), and (C)

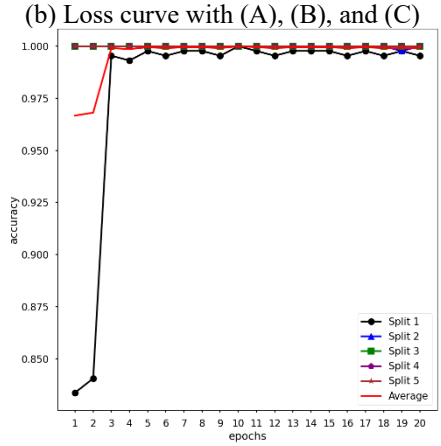

(c) Accuracy curve with (A)+(B) and (C)

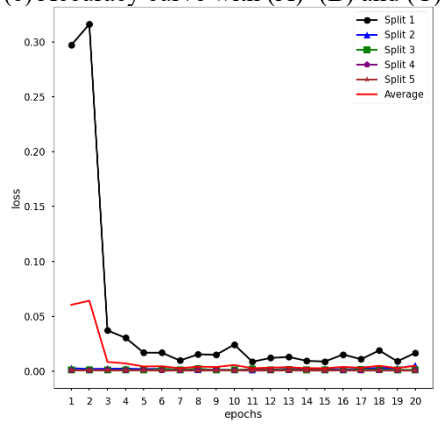

(d) Loss curve with (A)+(B) and (C)

Fig. 12 Learning curve of CNN

Table 2 CNN architecture

Input image (size)	GMW (217x217)
Stratified K-fold	K = 5
1. Convolution Layer	Number of Filters (64) Size of Filter (3x3) Stride Value (1) Activation (ReLU) Batch Normalization
2. Max Pooling Layer	Number of Filters (1) Size of Filter (2x2) Stride Value (1) Drop-out (0.25)
3. Convolution Layer	Number of Filters (128) Size of Filter (3x3) Stride Value (1) Activation (ReLU) Batch Normalization
4. Max Pooling Layer	Number of Filters (1) Size of Filter (2x2) Stride Value (1) Drop-out (0.25)
5. Fully Connected Layer	Activation (ReLU) Dense (256) Batch Normalization Drop-out (0.25)
6. Fully Connected Layer	Activation (SoftMax) Dense (2 or 3)
7. Compile	Optimizer (adagrad) Loss Function (sparse categorical crossentropy)

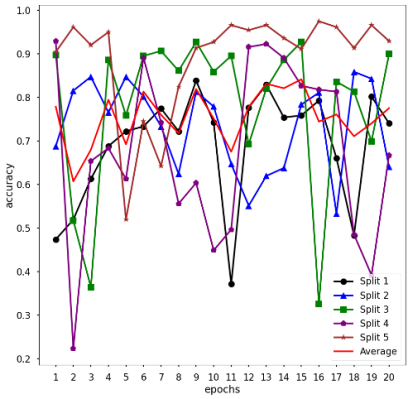

(a) Accuracy curve with (A), (B), and (C)

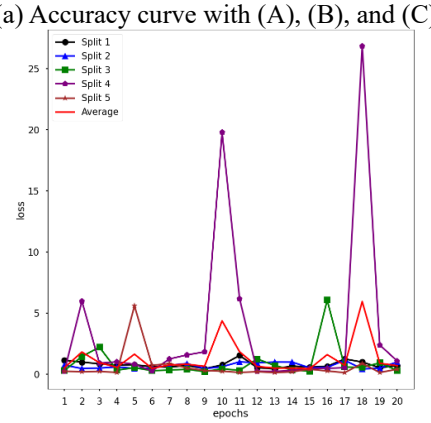

(b) Loss curve with (A), (B), and (C)

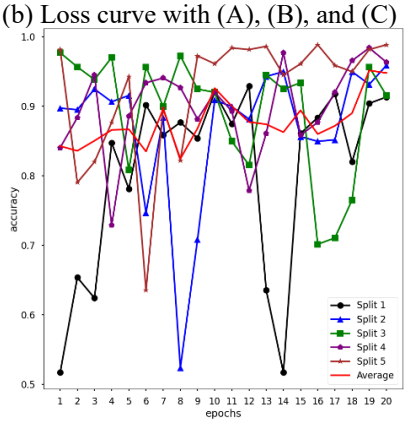

(c) Accuracy curve with (A)+(B) and (C)

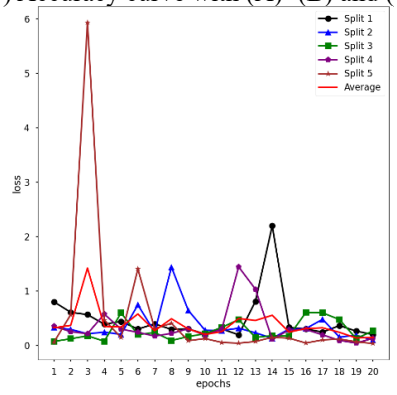

(d) Loss curve with (A)+(B) and (C)

Fig. 13 Learning curve of 1D-CNN

Fig. 13 confirms that learning did not proceed correctly under unstable progress. Therefore, finding a pattern that can distinguish defects in the time series data is tedious. On the other hand, the learning curves in Fig. 12 exhibit stable progress.

Moreover, the learning model confirms the robustness of the model, which refers to the degree to which the performance of a model changes when using test versus training data.

The performances of our model in CNN (with CWT image) and 1D-CNN were tested under two scenarios. The first involves classifying (A) with no flaw and possible boundary effect, (B) with no flaw, and (C) with a flaw, whereas the second involves classifying two categories (A)+(B) without flaws and (C) with a flaw.

In the evaluation of classification models, we employ both accuracy and the F1 score as performance metrics. These metrics are particularly useful for addressing the issue of imbalanced data. The results of applying the test data to the learning model are documented in Table 3. For clarity, accuracy measures the proportion of correct predictions and is calculated using the formula: (TP + TN) / (TP + TN + FP + FN), Precision represents the accuracy of positive predictions and is calculated as TP / (TP + FP), and Recall indicates how many of the actual positive cases were correctly identified, calculated as TP / (TP + FN), where True Positives (TP) are cases correctly identified as positive, True Negatives (TN) are cases correctly identified as negative, False Positives (FP) are negative cases incorrectly labeled as positive, and False Negatives (FN) are positive cases incorrectly labeled as negative. The F1-Score is the harmonic mean of Precision and Recall.

Table 3 Indicators of models using test data

CNN (C/B/A)	Test Data			
	Accuracy	Precision	Recall	F1-score
Split 1	0.954	0.942	0.937	0.939
Split 2	0.959	0.955	0.937	0.943
Split 3	0.964	0.951	0.953	0.952
Split 4	0.968	0.958	0.957	0.958
Split 5	0.961	0.946	0.952	0.948
Average	0.961	0.950	0.947	0.948
CNN (C/A+B)	Test Data			
	Accuracy	Precision	Recall	F1-score
Split 1	0.999	0.999	0.999	0.999
Split 2	0.998	0.998	0.998	0.998
Split 3	0.998	0.998	0.998	0.998
Split 4	0.999	0.999	0.999	0.999
Split 5	0.998	0.998	0.998	0.998
Average	0.998	0.998	0.998	0.998
1D-CNN (C/B/A)	Test Data			
	Accuracy	Precision	Recall	F1-score
Split 1	0.694	0.718	0.609	0.584
Split 2	0.665	0.723	0.601	0.558
Split 3	0.855	0.840	0.840	0.818
Split 4	0.614	0.721	0.632	0.589
Split 5	0.843	0.820	0.806	0.809
Average	0.734	0.764	0.698	0.672
1D-CNN (C/A+B)	Test Data			
	Accuracy	Precision	Recall	F1-score
Split 1	0.925	0.924	0.925	0.925
Split 2	0.948	0.951	0.947	0.948
Split 3	0.886	0.899	0.883	0.885
Split 4	0.953	0.955	0.952	0.953
Split 5	0.978	0.978	0.978	0.978
Average	0.938	0.941	0.937	0.938

As illustrated in Table 3, the CNN model exhibits greater robustness compared to the 1D-CNN model. This is substantiated by the smaller variance in performance metrics across various data splits, highlighting the CNN model's superior stability.

6. Conclusions

The proposed model exhibits impressive performance: the accuracy is more than 0.96 for the classification of three categories and higher than 0.99 for the classification of two categories. Although the difference between classes A and B is seemingly small, the model still exhibits good performance even for classifying three categories. Additionally, it does not require further preprocessing, including removing noises. The results reveal that the continuous wavelet-transformed image of the signal contains very sophisticated information, which can be detected by CNN. In contrast, the original data itself cannot be detected by 1D-CNN.

We anticipate numerous practical applications for our technologies, including void detection of concrete structures such as concrete roads, building walls or underground structures such as tunnel segments, underpass or underground facilities for public utilities.

For commercialization, the model should be trained using field testing data rather than that obtained experimentally. However, the results demonstrate that the appropriate model based on a combination of CWT and CNN and trained with actual data will be essential for classifying signal data using the impact echo method.

Therefore, the proposed impact-echo method based on CWT and CNN is a robust tool for tunnel lining backfill void detection.

Acknowledgments

This work is supported by the Korea Agency for Infrastructure Technology Advancement(KAIA) grant funded by the Ministry of Land, Infrastructure and Transport (Grant 22TBIP-C162312-02).

References

Aggelis, D., Shiotani, T. and Kasai, K. (2008), "Evaluation of grouting in tunnel lining using impact-echo", *Tunn. Undergr. Sp. Tech*., **23**(6), 629–637. https://doi.org/10.1016/j.tust.2007.12.001.

Cao, R., Ma, M., Liang, R. and Niu, C. (2019), "Detecting the void behind the tunnel lining by impact-echo methods with different signal analysis approaches", *Appl. Sci*., **9**(16), 3280. https://doi.org/10.3390/app9163280.

Carino, N.J. (2001), "The Impact-Echo Method: An Overview." Structures 2001. https://doi.org/10.1061/40558(2001)15.

Gong, C., Ding, W., Soga, K. and Mosalam, K. (2019), "Failure mechanism of joint waterproofing in precast segmental tunnel linings". *Tunn. Undergr. Sp. Tech*., **84**, 334-352. https://doi.org/10.1016/j.tust.2018.11.003.

He, K., Zhang, X., Ren, S. and Sun, J. (2016), "Deep residual learning for image recognition", *Proceedings of the 2016 IEEE Conference on Computer Vision and Pattern Recognition (CVPR)*. https://doi.org/10.1109/cvpr.2016.90.

Kwak, N.S. and Ko, T.Y. (2022), "Machine learning-based regression analysis for estimating Cerchar abrasivity index", *Geomech. Eng*., **29**(3), 219-228. https://doi.org/10.12989/gae.2022.29.3.219.

Lee, J.S., Park, J., Kim, J. and Yoon, H.K. (2022), "Study of oversampling algorithms for soil classifications by field velocity resistivity probe", *Geomech. Eng*., **30**(3), 247-258. https://doi.org/10.12989/gae.2022.30.3.247.

Liao, Y., Zeng, X. and Li, W. (2017), "Wavelet transform based convolutional neural network for gearbox fault classification", *Proceedings of the 2017 Prognostics and System Health Management Conference (PHM-Harbin)*. https://doi.org/10.1109/phm.2017.8079274.

Lilly, J.M. (2017), "Element analysis: a wavelet-based method for analysing time-localized events in noisy time series", *Proceedings of the Royal Society A: Mathematical, Physical and Engineering Sciences*, **473**(2200), 20160776. https://doi.org/10.1098/rspa.2016.0776.

Lilly, J.M. and Olhede, S.C. (2010), "On the analytic wavelet

transform", *IEEE T. Inform. Theory*, **56**(8), 4135-4156. https://doi.org/10.1109/tit.2010.2050935.
Lilly, J.M. and Olhede, S.C. (2012), "Generalized morse wavelets as a superfamily of analytic wavelets", *IEEE T. Signal Process*., **60**(11), 6036-6041. https://doi.org/10.1109/tsp.2012.2210890.
Lilly, J. and Olhede, S. (2009), "Higher-order properties of analytic wavelets", *IEEE T. Signal Process*., **57**(1), 146-160. https://doi.org/10.1109/tsp.2008.2007607.
Liu, N., Li, N., Xu, C., Li, G., Song, G. and Yang, M. (2020), "Mechanism of secondary lining cracking and its simulation for the dugongling tunnel", *Rock Mech. Rock Eng*.. **53**. 4539-4558.
Mirzaeiabdolyousefi, M., Nikkhah, M. and Zare, S. (2022), "Assessment of time-dependent behaviour of rocks on concrete lining in a large cross-section tunnel", *Geomech. Eng*., **29**(1), 41-51. https://doi.org/10.12989/gae.2022.29.1.041.
Moon, J., An, J., Kim, H., Lee, J. and Lattner, T. (2022), "Evaluation criteria for freezing and thawing of tunnel concrete lining according to theoretical and experimental analysis", *Geomech. Eng*., **29**(3). 349-357. https://doi.org/10.12989/gae.2022.29.3.349.
Sansalone, M.J. and Streett, W.B. (1997), "Impact-echo: nondestructive evaluation of concrete and masonry", Bullbrier Press:Jersey Shore, PA, USA.
Sasmal, S. and Behera, R. (2021), "Application of artificial intelligence methods for predicting transient response of foundation", *Geomech. Eng*., **27**(3), 197-211. https://doi.org/10.12989/gae.2021.27.3.197.
Sawicki, B., Piotrowski, T. and Garbacz, A. (2021), "Development of impact-echo multitransducer device for automated concrete homogeneity assessment", *Materials*, **14**(9), 2144. https://doi.org/10.3390/ma14092144.
Slavič, J., Simonovski, I. and Boltežar, M. (2003), "Damping identification using a continuous wavelet transform: Application to real data", *J. Sound Vib*., **262**(2), 291-307. https://doi.org/10.1016/s0022-460x(02)01032-5.
Song, K.I. and Cho, G.C. (2009), "Bonding state evaluation of tunnel shotcrete applied onto hard rocks using the impact-echo method", *NDT &Amp E Int*., **42**(6), 487-500. https://doi.org/10.1016/j.ndteint.2009.02.007.
Song, K.I. and Cho, G.C. (2010), "Numerical study on the evaluation of tunnel shotcrete using the impact-echo method coupled with fourier transform and short-time fourier transform", *Int. J. Rock Mech. Min. Sci*., **47**(8), 1274-1288. https://doi.org/10.1016/j.ijrmms.2010.09.005.
Xu, G., He, C., Wang, J. and Chen, Z. (2020), "Study on the mechanical behavior of a secondary tunnel lining with a yielding layer in transversely isotropic rock stratum", *Rock Mech. Rock Eng.*, **53**, 2957-2979. https://doi.org/10.1007/s00603-020-02107-1.
Yao, F., Chen, G. and Abula, A. (2018), "Research on signal processing of segment-grout defect in tunnel based on impact-echo method", *Constr. Build. Mater*., **187**, 280-289. https://doi.org/10.1016/j.conbuildmat.2018.07.192.